

Self-gravitating fluid dynamics, instabilities and solitons

B. Semelin^(a), N. Sánchez^(a), H. J. de Vega^(b)

(a) *Observatoire de Paris, Demirm, 61, Avenue de l'Observatoire, 75014 Paris, FRANCE. Laboratoire Associé au CNRS UA 336, Observatoire de Paris et École Normale Supérieure.*

(b) *Laboratoire de Physique Théorique et Hautes Energies, Université Paris VI, Tour 16, 1er étage, 4, Place Jussieu 75252 Paris, Cedex 05, FRANCE. Laboratoire Associé au CNRS UMR 7589*

(December 2, 2024)

This work studies the hydrodynamics of self-gravitating compressible isothermal fluids. We show that the hydrodynamic evolution equations in absence of viscosity are scale covariant. We study the evolution of the time dependent fluctuations around singular and regular isothermal spheres. We linearize the fluid equations around such stationary solutions and apply Laplace transform to solve them. We find that the system is stable below a critical size ($X \sim 9.0$ in dimensionless variables) and unstable above; this size is the same critical size found in the study of the thermodynamical stability in the canonical ensemble and associated to a center-to-border density ratio of 32.1. We prove that the value of this critical size is independent of the Reynolds number of the system. Furthermore, we give a detailed description of the series of successive dynamical instabilities that appear at higher and higher sizes following the geometric progression $X_n \sim 10.7^n$. We turn then to study exact solutions of the hydrodynamic equations without viscosity and we provide analytic and numerical axisymmetric soliton-type solutions. The stability of exact solutions corresponding to a collapsing filament is studied by computing linear fluctuations. Radial fluctuations growing faster than the background are found for all sizes of the system. However, a critical size ($X \sim 4.5$) appears, separating a weakly from a strongly unstable regime.

I. INTRODUCTION AND RESULTS

Understanding the dynamics of self-gravitating fluids is a fundamental issue in astrophysics. The fractal structure of the interstellar medium as well as the formation and evolution of cosmological structures are based on it. Compressible self-gravitating fluid mechanics plays a key role in both star formation and in the formation of a fractal structure for the interstellar medium [1].

Self-gravitating systems can be studied at different levels. The first is purely thermodynamical. It leads to the description of their states of equilibrium and the study of their stability. This approach has been followed in the case of the isothermal sphere configuration [2–6] leading to the description of the gravothermal instability. This behaviour appears when the size of the sphere goes above a critical size, or for a given size when its temperature goes below a critical temperature. An instability develops and the system collapses to a dense core. In refs. [9–12] the statistical mechanics of the self-gravitating gas has been investigated with analytic (saddle point on the functional integral) as well as Monte Carlo methods. In addition to the thermodynamics, this approach provides the exact equation of state of the self-gravitating gas [12].

The dynamics can be studied from the hydrodynamical equations of a self-gravitating fluid. This is a set of nonlinear partial differential equations and exact solutions can only be found under simplifying hypotheses. For example, the case of one space dimension has been studied in ref. [13] and the cylindrically symmetric case in ref. [14].

The last approach is numerical, it has been widely followed [8].

In this paper we study the hydrodynamics of a self-gravitating fluid. We show that the hydrodynamical evolution equations for a self-gravitating fluid are **covariant under scale transformations** in absence of viscosity. That is, if we scale the space and time variables by a constant factor on a solution of the fluid equations, we get again a solution of the equations.

We consider the Navier-Stokes equations for an isothermal self-gravitating fluid and restrict our study to potential flows. Within these hypothesis we show that a Reynolds number appears as the only parameter that breaks the scale covariance in the Navier-Stokes equations. Moreover we find that a characteristic density enters the Reynolds number definition, implying that a system with no characteristic density has no characteristic Reynolds number; the flow is then scale covariant.

In section III we present a general Laplace transform method for the linear dynamical stability analysis of stationary solutions of the equations.

In order to apply this analysis to isothermal spheres, we first specify the initial data and the boundary conditions. In section IV, using the Laplace transform, we derive the analytical form of the fluctuations in the case of a singular isothermal sphere background. Then, we show that the boundary conditions build a discret spectrum of proper

modes for the system. The stability of these modes is decided by the complex value of their pulsations in the Laplace transform plane. We then apply a general numerical method based on finite differences to both the singular and the regular isothermal sphere cases and compute the pulsations as functions of the size of the system. We show that in both the singular and the regular cases the dynamical stability depends on the size of the system. Under a critical size X_{c_1} the system is stable, while above it becomes unstable. In dimensionless variables this size is $X_{c_1} \sim 10.7\delta$ in the singular case (δ is the short distance cutoff necessary in this case) and $X_{c_1} \sim 9.0$ in the regular case. This critical size is the same as the one found in thermodynamical studies in the canonical ensemble (we used boundary conditions connected to the canonical ensemble). It is often expressed as a critical center-to-border density contrast whose value is 32.1 for the regular isothermal sphere. However, we also show how secondary instabilities X_{c_2}, \dots, X_{c_n} appear at larger sizes. These sizes follow the geometric progression 10.7^n ($n = 1, 2, \dots$) in the singular case and do so asymptotically ($n \gg 1$) in the regular case. The density and velocity profiles of the two first instabilities are given. Figs. 1-3 show these profiles and the spectrum of modes for the regular and singular spheres.

In section V we include the viscosity in the fluid equations. Then, we study the influence of the Reynolds number on the stability criterion. The result is that the critical sizes at which the unstable modes appear are **independent** of the Reynolds number. The complex evolution of the pulsations of the modes as functions of both the system size and the Reynolds number is plotted in figs. 4-6.

In section VI we turn to more complex background solutions. We look for axisymmetric soliton-type solutions. We define a soliton variable:

$$y = \frac{\mu r}{1 \pm \mu c_s t}, \quad (1.1)$$

where μ is an inverse characteristic length (μ^{-1} is the Jeans' length), c_s the sound speed, r the polar radius and t the time. We reduce the equations to a single non-linear equation and we find non-trivial solutions such as,

$$v_r = \pm c_s \left(\sqrt{C} + \frac{\mu r}{1 \pm \mu c_s t} \right), \quad \phi = \ln \left[\frac{\sqrt{C}}{\mu^2 r^2 (1 \pm \mu c_s t)} \right]. \quad (1.2)$$

This solution describes an expanding or collapsing filament depending on the choice for \pm . Other background solutions are described. Then, explicit radial fluctuations around the solution (1.2) are computed and their stability is analyzed with the same method as for the isothermal spheres. Some of the modes appear to grow faster than the background whatever the size of the system. A specific size, $X_{c_1} \sim 4.5\delta$, marks the appearance of faster growing fluctuations at larger sizes. However, these are only radial fluctuations invariant along the axis of the symmetry; this means that they have an infinite mass for all radial sizes of the system. Limitating the size of the system along the symmetry axis should provide a stable behaviour for small enough sizes.

In section VII we give our conclusions and final remarks.

II. THE NAVIER-STOKES EQUATION FOR SELF-GRAVITATING FLUIDS

The evolution of a self-gravitating, isothermal fluid is described by a density field, $\rho(\mathbf{r}, t)$, a pressure field $P(\mathbf{r}, t)$, a gravitational potential $U(\mathbf{r}, t)$ and a velocity field $\mathbf{v}(\mathbf{r}, t)$. These four fields obey four equations: the matter conservation, the Navier-Stokes equation, the Poisson equation and the equation of state [7], respectively given by

$$\frac{\partial \rho}{\partial t} + \nabla \cdot (\rho \mathbf{v}) = 0, \quad (2.1)$$

$$\frac{\partial \mathbf{v}}{\partial t} + (\mathbf{v} \cdot \nabla) \mathbf{v} = -\frac{\nabla P}{\rho} - \nabla U + \frac{\eta}{\rho} \nabla^2 \mathbf{v} + \frac{1}{\rho} \left(\zeta + \frac{\eta}{3} \right) \nabla (\nabla \cdot \mathbf{v}), \quad (2.2)$$

$$\nabla^2 U = -4\pi G \rho, \quad (2.3)$$

$$c_s^2 = \frac{\partial P}{\partial \rho}. \quad (2.4)$$

Here ζ and η stand for the kinematical viscosity and c_s is the speed of sound. From now on we restrict ourselves to potential flows, which implies the existence of a velocity potential ψ . In order to work with dimensionless variables we define μ , the inverse of a characteristic length, as:

$$\mu^2 = \frac{4\pi G \rho_0}{c_s^2}. \quad (2.5)$$

where ρ_0 is a characteristic density of the system.

We then introduce dimensionless variables and fields :

$$\begin{aligned} \mathbf{x} &= \mu \mathbf{r} \quad , \quad \tau = \mu c_s t \quad , \\ \phi &= \ln \frac{\rho}{\rho_0} \quad , \quad \mathbf{v} = \frac{c_s}{\mu} \nabla_{\mathbf{x}} \psi(\mathbf{x}, \tau) \quad . \end{aligned} \quad (2.6)$$

Here, $\nabla_{\mathbf{x}}$ is the derivative with respect to the dimensionless coordinate \mathbf{x} . We can take advantage of the potential nature of the velocity field to simplify the dissipation term in the Navier-Stokes equation. Taking the divergence of the Navier-Stokes equation and eliminating the equation of state and the Poisson equation, the evolution equations can be written as

$$\partial_{\tau} \nabla^2 \psi + (\partial_{i,k} \psi)^2 + \partial_k \psi \partial_k \nabla^2 \psi = -\nabla^2 \phi - e^{\phi} + \frac{1}{Re} \nabla \cdot [e^{-\phi} \nabla (\nabla^2 \psi)] \quad , \quad (2.7)$$

$$\partial_{\tau} \phi + \nabla^2 \psi + \nabla \phi \cdot \nabla \psi = 0, \quad (2.8)$$

$$\frac{1}{Re} = \left(\frac{4}{3} \eta + \zeta \right) \frac{\mu}{\rho_0 c_s} \quad . \quad (2.9)$$

Sumation over repeated indices is implied. Moreover we used the notation:

$$(\partial_{i,k} f)^2 = (\partial_i \partial_k f)^2.$$

Re is the analogous of the usual Reynolds number for the compressible self-gravitating flow. We see now that in absence of a characteristic density in the system the flow is scale covariant. This can be proven as follows. Assume that $\{\phi(\mathbf{x}, \tau), \psi(\mathbf{x}, \tau)\}$ is a solution of eqs.(2.7)-(2.8). We then define the scale-transformed fields as

$$\begin{aligned} \phi_{\lambda}(\mathbf{x}, \tau) &= \phi(\lambda \mathbf{x}, \lambda \tau) + \ln \lambda^2 \quad , \\ \psi_{\lambda}(\mathbf{x}, \tau) &= \lambda^{-1} \psi(\lambda \mathbf{x}, \lambda \tau) \quad . \end{aligned} \quad (2.10)$$

Using now that

$$\begin{aligned} \frac{\partial \phi_{\lambda}}{\partial x_k} &= \lambda \frac{\partial \phi}{\partial y_k} \quad , \quad \frac{\partial \phi_{\lambda}}{\partial \tau} = \lambda \frac{\partial \phi}{\partial \tilde{\tau}} \\ \frac{\partial \psi_{\lambda}}{\partial x_k} &= \frac{\partial \psi}{\partial y_k} \quad , \quad \frac{\partial \psi_{\lambda}}{\partial \tau} = \frac{\partial \psi}{\partial \tilde{\tau}} \end{aligned} \quad (2.11)$$

where $y_k \equiv \lambda x_k$ and $\tilde{\tau} \equiv \lambda \tau$, we obtain that $\phi_{\lambda}(\mathbf{x}, \tau), \psi_{\lambda}(\mathbf{x}, \tau)$ is also a solution of eqs.(2.7)-(2.8) for $Re = \infty$. The transformation (2.10) generalizes to the time dependent case the scale transformation for $\phi(\mathbf{x})$ found in ref. [10] in the hydrostatic case.

We find from eqs.(2.6) and (2.10) that the velocity field transforms as,

$$\mathbf{v}_{\lambda}(\mathbf{x}, \tau) = \mathbf{v}(\lambda \mathbf{x}, \lambda \tau)$$

Under this transformation all terms are transformed as λ in eq.(2.8) and as λ^2 in eq.(2.7) except for the last (viscous) term that scales as λ . Therefore, for $\lambda \rightarrow \infty$ scale invariance is recovered. This corresponds to the long wavelength limit as one could expect.

When the flow is a fluctuation, for example, around an isothermal sphere with a characteristic central density, the scale invariance is broken. However, we will realize that scale invariance is recovered asymptotically at large distances in that case.

III. THE DYNAMICAL STABILITY OF ISOTHERMAL SPHERES

We study in this section the evolution of time dependent fluctuations around an isothermal sphere. We linearize the fluid equations (2.7)- (2.8) around such exact static solutions and apply Laplace transform to solve them.

A. Linearization

Equation (2.7) and (2.8) have well-known static spherically symmetric solutions: the isothermal spheres. These are the solutions to the equations:

$$\frac{d^2\phi_0}{dx^2} + \frac{2}{x} \frac{d\phi_0}{dx} + e^{\phi_0} = 0, \quad (3.1)$$

$$\psi_0 = 0, \quad (3.2)$$

where x is the dimensionless radius μr . These solutions are studied in [5]. Their thermodynamical stability has been extensively studied, leading to the discovery of the gravo-thermal instability ([2], [3] and [4]). Our aim is to investigate the dynamical instability of these states and compare with the thermodynamical results [12]. To achieve the stability analysis we introduce fluctuations around the isothermal spheres:

$$\phi_{tot} = \phi_0 + \epsilon \phi(\mathbf{x}, \tau) \quad (3.3)$$

$$\psi_{tot} = \epsilon \psi(\mathbf{x}, \tau) \quad (3.4)$$

where ϵ is a small parameter.

We can then write the linearized system where only first order contributions in ϵ are kept:

$$\partial_\tau \nabla^2 \psi(\mathbf{x}, \tau) = -\nabla^2 \phi(\mathbf{x}, \tau) - e^{\phi_0(x)} \phi(\mathbf{x}, \tau) + \frac{1}{Re} \nabla \cdot [e^{-\phi_0(x)} \nabla (\nabla^2 \psi(\mathbf{x}, \tau))], \quad (3.5)$$

$$\partial_\tau \phi(\mathbf{x}, \tau) + \nabla^2 \psi(\mathbf{x}, \tau) + \nabla \phi_0(x) \cdot \nabla \psi(\mathbf{x}, \tau) = 0. \quad (3.6)$$

Expanding $\psi(\mathbf{x}, \tau)$ and $\phi(\mathbf{x}, \tau)$ in spherical harmonics leads to a set of pairs of ordinary differential equations (ODE). Let us write first,

$$\phi(\mathbf{x}, \tau) = \sum_{l,m} \phi_{l,m}(x, \tau) Y_{l,m}(\theta, \phi), \quad (3.7)$$

$$\psi(\mathbf{x}, \tau) = \sum_{l,m} \psi_{l,m}(x, \tau) Y_{l,m}(\theta, \phi). \quad (3.8)$$

Then, the action of the laplacian is:

$$\nabla^2 = \frac{d^2}{dx^2} + \frac{2}{x} \frac{d}{dx} - \frac{l(l+1)}{x^2}. \quad (3.9)$$

Then, the radial parts of the expansions yield decoupled ODE labelled by l :

$$\begin{aligned} \nabla^2 \partial_\tau \psi_l(x, \tau) + [\nabla^2 + e^{\phi_0}] \phi_l(x, \tau) - \frac{1}{Re} [e^{-\phi_0} \nabla^2 \nabla^2 + \partial_x (e^{-\phi_0}) \partial_x \nabla^2] \psi_l(x, \tau) &= 0, \\ \partial_\tau \phi_l(x, \tau) + [\nabla^2 + (\partial_x \phi_0) \partial_x] \psi_l(x, \tau) &= 0. \end{aligned} \quad (3.10)$$

Analytic solutions will be given in specific cases. We analyze below these linear equations by using Laplace transformation in time, showing that this approach is the best for a stability analysis.

B. Laplace transform analysis

The Laplace transforms of our fields are defined by:

$$\hat{\phi}_l(x, s) = \int_0^{+\infty} d\tau e^{-s\tau} \phi_l(x, \tau),$$

$$\hat{\psi}_l(x, s) = \int_0^{+\infty} d\tau e^{-s\tau} \psi_l(x, \tau) . \quad (3.11)$$

The Laplace transform of the evolution equations (3.10) takes then the form

$$\begin{bmatrix} s \nabla^2 - \frac{1}{R} e^{-\phi_0(x)} \nabla^2 \nabla^2 - \frac{1}{R} \partial_x(e^{-\phi_0(x)}) \partial_x \nabla^2 & \nabla^2 + e^{\phi_0(x)} \\ \nabla^2 + \partial_x \phi_0 \partial_x & s \end{bmatrix} \begin{pmatrix} \hat{\psi}_l(x, s) \\ \hat{\phi}_l(x, s) \end{pmatrix} = \begin{pmatrix} \nabla^2 \psi_l(x, \tau = 0) \\ \phi_l(x, \tau = 0) \end{pmatrix} \quad (3.12)$$

This is a system of two linear ODE where s plays the role of a parameter. We specify boundary conditions at a finite distance. Therefore, the spectrum of the linear differential operator (3.12) becomes discrete. For particular values s_k of s , the determinant of the differential operator vanishes; the eigenvector of the one-dimensional kernel is then an eigenmode of the system associated to the pulsation s_k .

The fields follow by the inverse Laplace transforms

$$\begin{aligned} \phi_l(x, \tau) &= \int_{\Gamma} ds e^{s\tau} \hat{\phi}_l(x, s) , \\ \psi_l(x, \tau) &= \int_{\Gamma} ds e^{s\tau} \hat{\psi}_l(x, s) . \end{aligned} \quad (3.13)$$

where the contour Γ runs upwards parallel and to the right of the imaginary s axis. Closing the contour and computing the integral in eqs.(3.13) by residua we get for the fields a sum of terms associated to the poles of the integrand. That is, to the zeroes of the determinant of eq.(3.12). These terms depend on time through $e^{s_k \tau}$. If s_k has a positive real part the mode is unstable, growing exponentially with time.

The method for analyzing the stability of the system is now clear: we determine the zeroes of the determinant of our operator (3.12) as a function of s for various values of l and various boundary conditions, and we look for zeroes in the $\text{Re}(s) > 0$ half-plane of the complex s -plane.

C. Boundary conditions specifications

Different physical conditions justify different boundary conditions. In order to be able to compare our results with the thermodynamical approach we will choose conditions associated to the canonical ensemble formalism. We will confine our system in a spherical box of radius X . Within this box, we impose zero total mass for the perturbation of the density field, but a fluctuating energy. Along with regularity conditions, this leads to the following four constraints:

$$\begin{aligned} \int_0^X \phi(x, \tau) e^{\phi_0} x^2 dx &= 0 \quad , \quad \partial_x \phi(x, \tau)|_{x=0} = 0 \quad , \\ \partial_x \psi(x, \tau)|_{x=X} &= 0 \quad , \quad \psi(X, \tau) = 0 \quad . \end{aligned} \quad (3.14)$$

IV. THE NON-VISCOUS ISOTHERMAL SPHERES

A. Analytical study

The singular isothermal sphere is an analytical solution to eq (3.1) given by,

$$\phi_0 = \ln \frac{2}{x^2} . \quad (4.1)$$

This solution has an infinite total mass and produces infinite pressure at the center. To avoid this divergence we introduce a short distance cutoff δ . The spherical box provides the long distance cutoff. The advantage of such analytical solution is that we can write down analytical expressions for the fluctuations. Indeed for $l = 0$, eq.(3.12) reduces to:

$$\frac{d^2 f_s}{dx^2} + \left(\frac{2}{x^2} - s^2 \right) f_s(x) = 0 , \quad (4.2)$$

where $f_s(x) = \nabla\psi_0(x, s)$ is the dimensionless radial velocity of the $l = 0$ mode. In dimensionful variables, the radial velocity fluctuations for $l = 0$ are:

$$v_r(r, t) = c_s (A_1 e^{i\omega t} + A_2 e^{-i\omega t}) \sqrt{kr} [B_1 J_\nu(kr) + B_2 J_{-\nu}(kr)] ,$$

$$\omega^2 = k^2 c_s^2 \quad , \quad \nu = \frac{i\sqrt{7}}{2} . \quad (4.3)$$

where $J_\nu(z)$ are Bessel functions. The corresponding fluctuation $\phi(r, t)$ takes the form

$$\phi(r, t) = (A'_1 e^{i\omega t} + A'_2 e^{-i\omega t}) \sqrt{kr} \left[B'_1 \frac{dJ_\nu}{dr}(kr) + B'_2 \frac{dJ_{-\nu}}{dr}(kr) \right] . \quad (4.4)$$

The boundary conditions yield a system of four equations for the constants B_1, B_2, B'_1 and B'_2 . Non-zero solutions are possible when the determinant of this system is zero, which happens for specific values of k yielding a discrete spectrum for the modes. We have checked that the general method that we will describe in section IV B yields numerically the same results as eqs.(4.3)-(4.4). In both methods we need to adapt the boundary conditions to this singular case. We introduce the short distance cutoff δ :

$$\int_\delta^X \hat{\phi}_l(x, s) e^{\phi_0} x^2 dx = 0 \quad , \quad \partial_x \hat{\phi}_l(x, s) \Big|_{x=\delta} = 0 ,$$

$$\partial_x \hat{\psi}_l(x, s) \Big|_{x=X} = 0 \quad , \quad \hat{\psi}_l(X, s) = 0 . \quad (4.5)$$

The first condition is actually stronger than eq.(3.14) which implies this condition only for $l = 0$. However, we generalize the constraint for $l \neq 0$, this prevents a center of mass displacement.

B. Stability of the singular sphere

The general numerical method (which we will also use in the case of the regular isothermal sphere), consists in replacing the derivatives by finite differences turning eq.(3.12) and the boundary conditions into a $N \times N$ ($N \gg 1$) linear system. Non-zero solutions are found when the determinant of the system is zero. This happens for discrete values of the parameter s . If one of these eigenvalues s has a positive real part, then the associated mode grows with time and the system is unstable. It is known from thermodynamical studies that for a given central density, the stability depends on the size of the sphere. Thus, we will investigate for the zeroes of the determinant in a three-dimensional domain $(s, X) \in \mathbb{C} \times \mathbb{R}$. The zeroes are shown on fig.1 for $l = 0$.

The first point is that there is a symmetry around the $\text{Re}(s) = 0$ axis; we have a set of coupled modes with opposite pulsations. Then, we verified that the pulsations of the spectrum of modes have purely imaginary values for X smaller than a critical value X_{c_1} . This range of X values is mostly outside the domain pictured on fig.1 since behaviour of the system is simple there (however $\ln(X_{c_1} + 1) \sim 2.4$ is visible on the figures). In this regime the modes are oscillating stationary modes and the system is stable. As X increases above X_{c_1} , the size of the system grows and a first mode encounters a branching point and develops a real positive pulsation. This means that the mode grows exponentially and the system becomes unstable. Then, for successive critical values X_{c_i} , $i = 1, 2, \dots$ corresponding to larger and larger sizes of the system, new modes become unstable. It is interesting to mention that the critical values appear when the rate of the larger and lower cutoffs is $X_{c_n}/\delta \sim 10.7^n$. This geometric progression has been found in the thermodynamical study in ref. [11].

Non-radial perturbations have been investigated ($l \neq 0$). These perturbations are always stable and oscillating. The case $l = 1$ could show a pseudo-instability associated with an overall translation of the system, but such mode is excluded by our choice of boundary conditions.

C. Stability of the regular isothermal spheres

Regular solutions of eq.(3.1) have been widely studied in spite of the fact that they do not have an analytical expression. In this case it is not necessary to introduce a short distance cutoff in the study of the fluctuations since the background solution is regular at the origin. We keep considering the solution in a large but finite sphere of radius X . Thus we will use the same boundary conditions as in the singular case, taking $\delta = 0$.

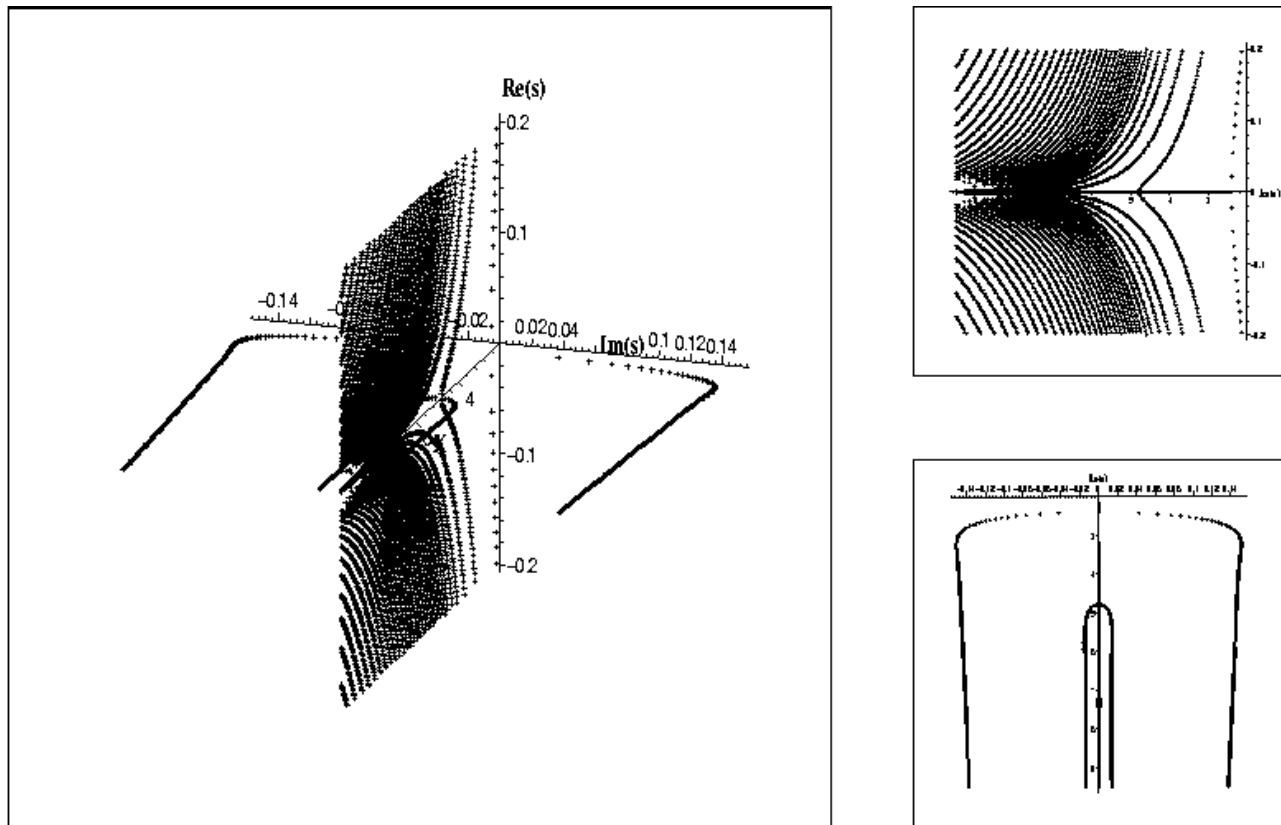


FIG. 1. Spectrum of the modes around the singular isothermal sphere. The real and imaginary parts of the pulsations of the modes are plotted in the 3d-view for a range of values of the size X . All scales are **logarithmic** ($\ln(1+x)$ actually). Views from the right and from above are also plotted.

We again apply the general numerical method described above. We compute the spectrum of pulsations of the modes for varying values of the size X of the sphere (see fig.2).

The first point is that the behaviour is very similar to the singular case. The interpretation of fig.2 is the same as that of fig.1. This means that the singular isothermal sphere with short distance cutoff is a good analytical analogue of the regular isothermal sphere. The only difference in the behaviour of the fluctuations is in the specific values of the X_{c_i} . In the regular case, the instability appears at a smaller size ($X_{c_1} \sim 9.$) than in the singular case ($X_{c_1} \sim 10.7$). The value in the singular case is given for $\delta = 1$ since the actual parameter is the ratio $\frac{X}{\delta}$. As expected, the value $X_{c_1} \sim 9.0$ corresponds to a ratio of 32.1 between the central and border densities of the background. This critical ratio is the same as in the study of the thermodynamical stability in the canonical ensemble [4]. Finally the numerical study suggests that the ratio 10.7 between two successive X_{c_i} is asymptotically obtained at large X in the regular case, as it must be.

D. Profile of the instable modes

Having established that the dynamical instability appears for the same center-to-border density contrast as in the thermodynamical instability, we now check if the profile of the first instable mode matches the profile of the thermodynamical instability, and we investigate the profile of other instable modes.

Those profiles are given, when we use the finite differences method, by the coordinates of the vector of the one-dimensional kernel of our operator. For a given size, we are thus able to determine the profile of each mode associated with a zero of the determinant for specific values of s . On fig. 3 the profiles are given for the first and second instabilities for sizes just above their critical sizes. As can be seen, the first instability is a spherical collapse forming a dense core. Its density profile is similar to the profile of the thermodynamical instability [6]. The second instability combines a core collapse and the ejection of a shell.

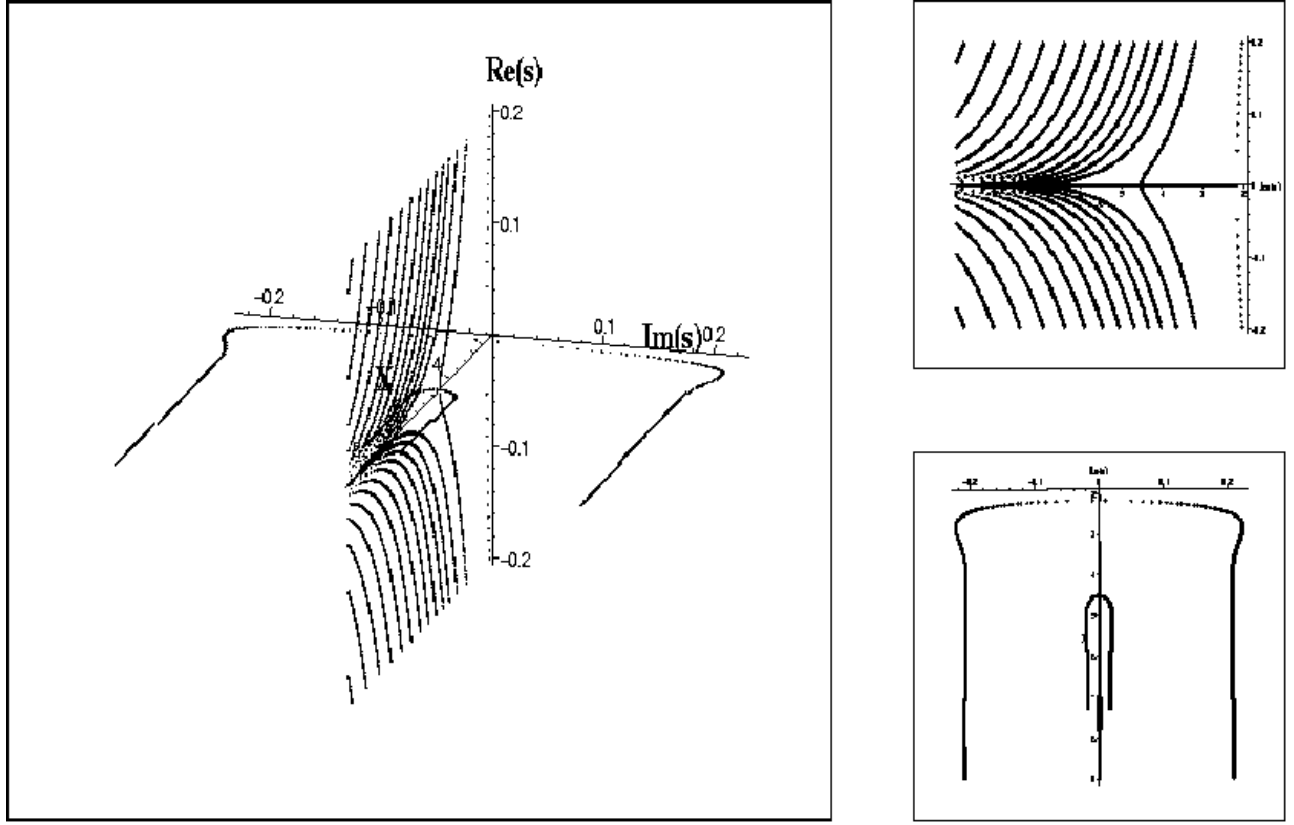


FIG. 2. Spectrum of the modes around the regular isothermal spheres. Explanations are the same as in Fig 1.

V. EFFECT OF VISCOSITY ON THE DYNAMICS AND STABILITY CRITERIA

It is now interesting to establish how viscosity alters the dynamics of the fluctuations. We first proceed to an analytic study of the fluctuations and then perform a thorough numerical analysis.

A. Analytical study

Here we will study the fluctuations around the singular isothermal sphere with a non-zero viscosity. We consider only radial perturbations since it simplifies the equations and contains the essential information about stability. Using the variables:

$$y = s x , \quad f(y) = \nabla\psi(sx), \quad (5.1)$$

where f is the (dimensionless) radial velocity, the system (3.12) becomes

$$\left(1 + \frac{1}{s Re} \frac{y^2}{2}\right) \frac{d^2 f}{dy^2} + \frac{y}{s Re} \frac{df}{dy} + \left(\frac{2}{y^2} - 1\right) f = 0 . \quad (5.2)$$

It is interesting to notice that all the dependence on the parameters is through the combination $s Re$. The asymptotic behaviour of the solutions at large distance is:

$$y \gg 1 , \quad y \gg s Re : \quad f(y) = y^{\frac{-1 \pm \sqrt{1 + 8 s Re}}{2}} . \quad (5.3)$$

For positive s , that is, solutions growing exponentially with time, the solution with the upper sign grows at large radii while the other solution decays. For negative s , both solutions decay. The interval $0 > s Re > -1/8$ is the

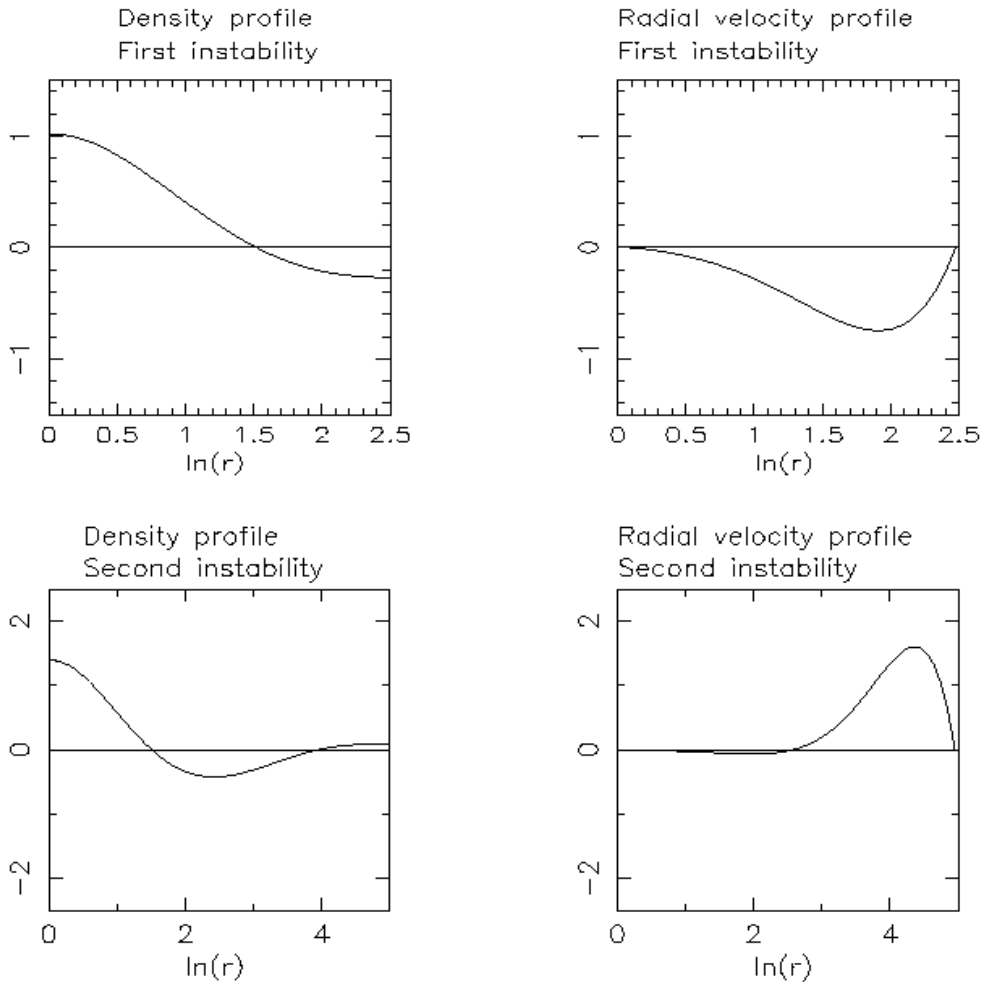


FIG. 3. Radial profiles of the first two instabilities, at sizes just above their emergence, plotted for arbitrary amplitudes.

only range giving strictly decaying behaviours at large radii. In the other cases ($sRe < -1/8$ or s complex) we have spatially oscillating and decaying behaviours. It is easy to check that at small distances one recovers the zero-viscosity solutions. This, of course, does not take the boundary conditions into account. We provide in the next section quantitative results from numerical calculations.

B. Numerical study

The introduction of the viscosity, although formally cumbersome, fits with no particular difficulty in the finite difference scheme. The spectrum of modes for a continuous range of the larger cutoff X can be computed for different values of the Reynolds number. These results are shown on fig.4 and fig.5. We show in fig.6 the evolution of the spectrum at fixed sizes, for a continuous range of values of the Reynolds number.

Obviously, the diagrams are more complex in the viscous case than in the ideal case, especially as we go to Reynolds numbers close to one. Reynolds numbers as small as 0.1 have been investigated but are not plotted since they show no specificity and are unlikely values for a self-gravitating gas. We have three main kind of modes: oscillating-decaying modes, decaying modes, and growing modes. However, all the values of the critical sizes associated with the onset of instabilities are **independent** of the Reynolds number. This can be guessed on fig.5, and checked on fig 6 for X_{c1} . The stability of the isothermal sphere **does not depend** on the viscosity. Besides, figs.4 and 5 clearly show that the mode associated with the first instability is much less affected by the viscosity than the others.

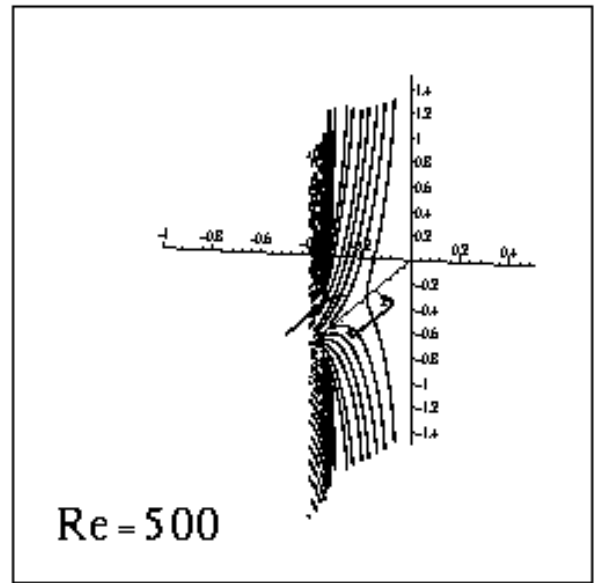
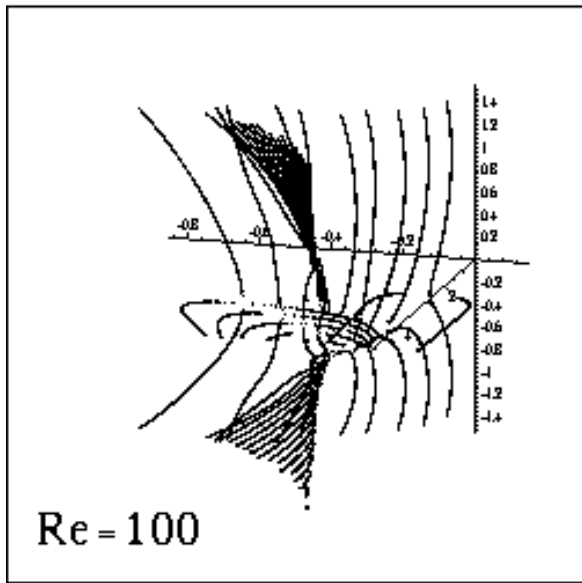
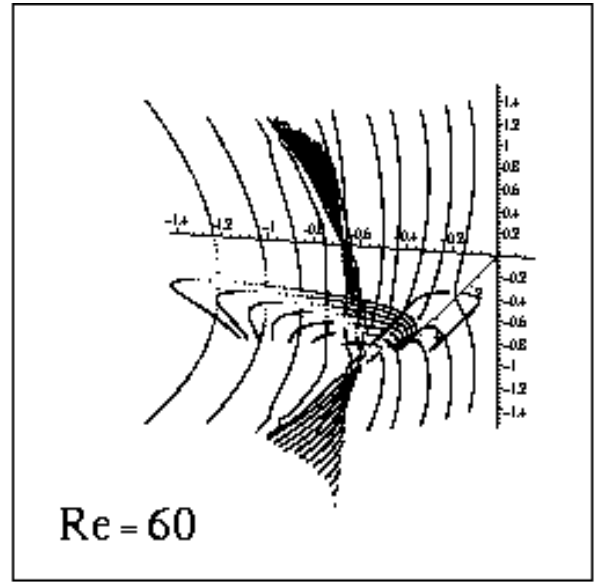
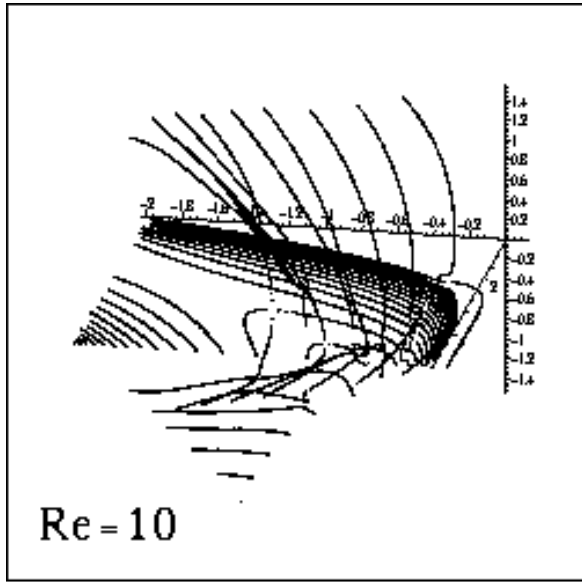


FIG. 4. Spectrum of viscous modes around the singular isothermal sphere. The real and imaginary parts of the pulsations of the modes are plotted in 3d-views for a range of values of the size X , and four values of the Reynolds number. All scales are logarithmic.

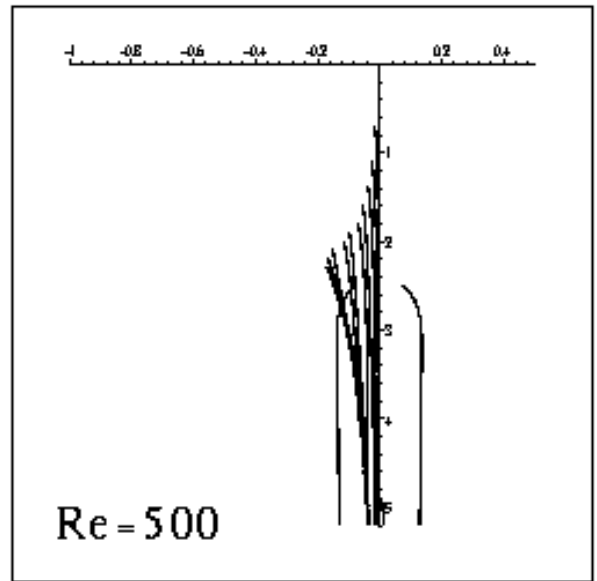
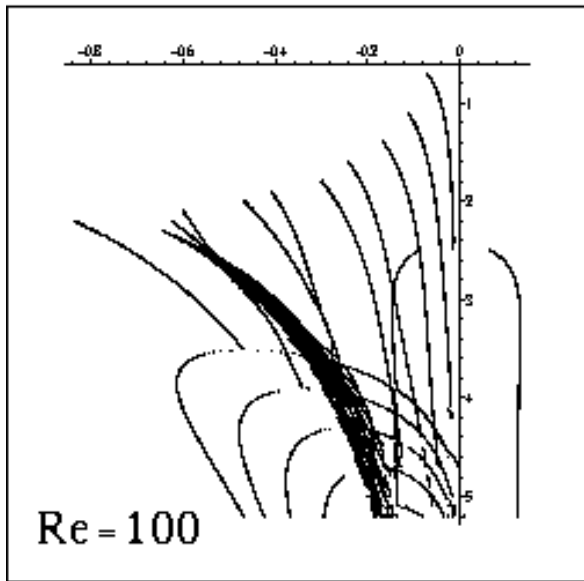
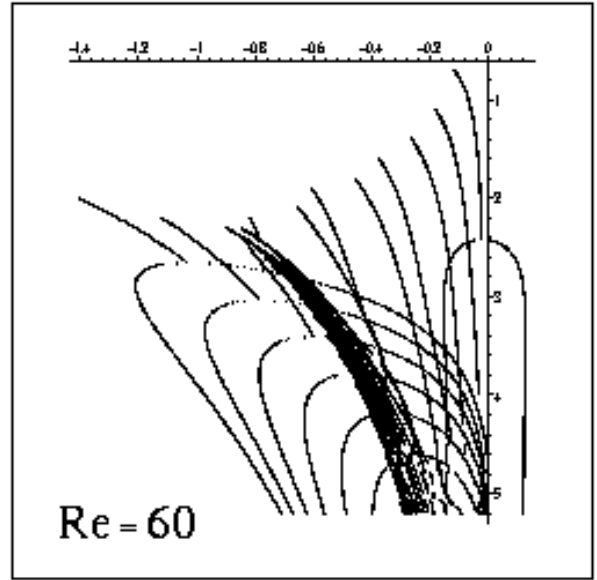
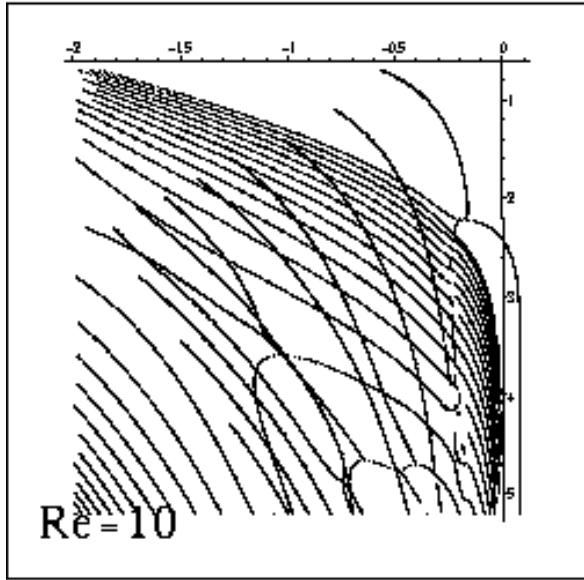


FIG. 5. Upper views of fig. 4. The real parts of the pulsations of the modes appear as functions of the size X . Positive real parts appear for the same values of X ($\ln(1 + X) \sim 2.4$), independently of the Reynolds number.

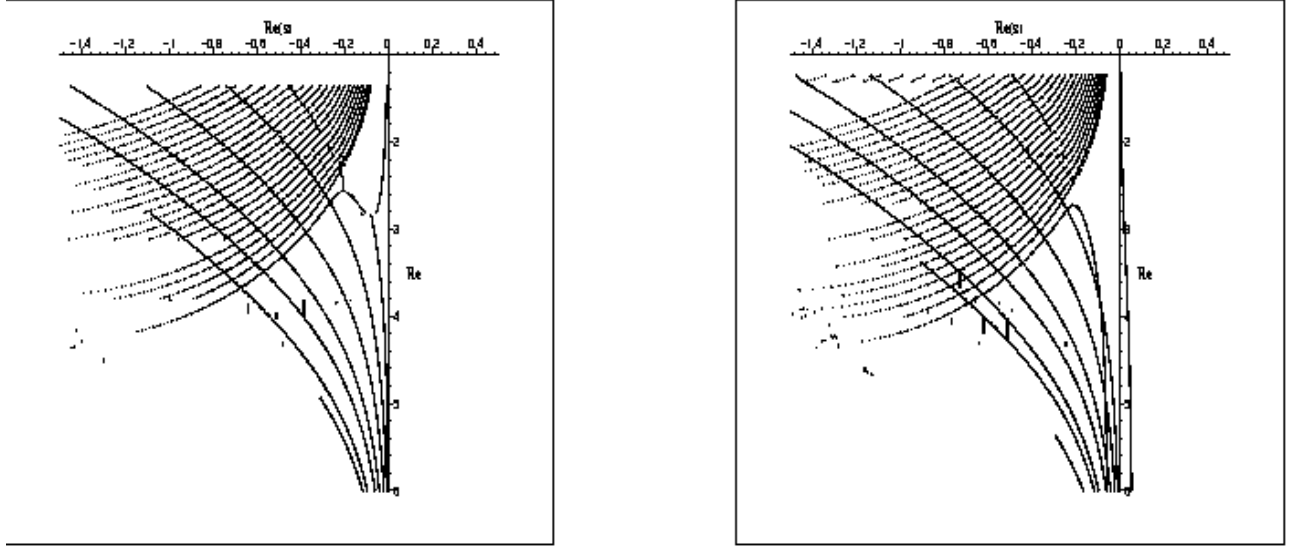


FIG. 6. The real parts of the pulsations of the modes are plotted as functions of the logarithm of the Reynolds numbers for fixed size: 10.5 on the left and 11.6 on the right.

The real parts of the modes are plotted on fig.6 as functions of the Reynolds number with logarithmic scales, for two different sizes: 10.5 and 11.6 . In the first diagram all modes are stable independently of the Reynolds number and in the second there is exactly one unstable mode for all values of the Reynolds number. This is a confirmation that the dynamical stability criterion depends only on the size of the system and not on the value of the Reynolds number.

VI. SOLITON-TYPE SOLUTIONS IN THE SELF-GRAVITATING GAS

The appearance of solitons in an isothermal self-gravitating gas has been studied in one spatial dimension in ref. [13]. In this case, the system could be reduced to a sine-Gordon equation. Here we will study the case of axisymmetric soliton-type solutions in $3 + 1$ dimensions.

A. Soliton-type equations

We will consider z -independent solutions to the evolution equations (2.7)-(2.9) without viscosity ($Re = \infty$). It is useful to make the following change of variables,

$$(r, t) \longrightarrow \left(y = \frac{r}{r_0(t)}, t \right), \quad (6.1)$$

where $r_0(t)$ is a time dependent characteristic length. The simplest non-trivial choice for $r_0(t)$ is a linear dependence on time. Using the characteristic parameters of the system this leads the soliton variable:

$$y = \frac{\mu r}{1 \pm \mu c_s t} = \frac{x}{1 \pm \tau}. \quad (6.2)$$

We write the potential and radial velocity field as:

$$\phi = \ln \left[\frac{f(y)}{(1 \pm \tau)^2} \right], \quad \frac{d\psi}{dx} = h(y) \pm y. \quad (6.3)$$

Then, the matter conservation equation (2.8) yields

$$\frac{h'(y)}{h(y)} + \frac{1}{y} + \frac{f'(y)}{f(y)} = 0, \quad ,$$

which can be immediately integrated as

$$f(y) h(y) y = \mp C . \quad (6.4)$$

The symbol \mp in front of C is introduced for later convenience. Each possibility is associated with one of the choices for the soliton variable. C going to zero means that the density goes to zero. Inserting eqs.(6.3) and (6.4) in the Euler equation of motion (2.7) gives the non linear equation:

$$h \left(y \left(hh' \pm h - \frac{h'}{h} \right) \right)' = \pm C . \quad (6.5)$$

It is possible to derive some analytical solutions to this equation.

B. Analytical solutions

The simplest solution to eq.(6.5) is $h(y) = \mp \sqrt{C}$. In terms of physical fields this produces non-trivial solutions:

$$\psi' = \pm c_s \left(-\sqrt{C} + \frac{r}{\mu^{-1} \pm c_s t} \right) , \quad \phi = \ln \left[\frac{-\sqrt{C}}{\mu^2 r^2 (1 \pm \mu c_s t)} \right] = \ln \frac{2}{x^2} + \ln(\sqrt{C} y) . \quad (6.6)$$

These two solutions are filaments, one expanding and the other collapsing in a finite time. This solution is invariant under the following scale transformations

$$C \longrightarrow \lambda C , \quad c_s \longrightarrow \frac{c_s}{\lambda} , \quad \mu \longrightarrow \lambda \mu . \quad (6.7)$$

Hence, in the calculation of the fluctuations [sec. VI C], we can set for example $\sqrt{C} = 1$.

Guided by numerical integration (see fig. 7), another type of solution can be found for low densities. It is possible to build a perturbative solution of eq.(6.5) around the exact solution $C = 0$, $h(y) = \mp y$. Since the system is ill-defined at $C = 0$, we will consider $C \ll 1$ and we will develop $h(y)$ perturbatively in C .

$$h(y) = \mp y [1 + C h_1(y) + \mathcal{O}(C^2)] . \quad (6.8)$$

Then $h_1(y)$ obeys the simple equation:

$$y^2 h_1 + y(y^2 - 1) h_1' = \pm \ln \frac{B}{y} , \quad (6.9)$$

which has the general solution,

$$h_1(y) = \frac{1}{\sqrt{|y^2 - 1|}} \left(A \pm \int \frac{dy \ln \left(\frac{B}{y} \right)}{y \sqrt{|y^2 - 1|}} \right) . \quad (6.10)$$

We see that in general $h_1(y)$ is singular at $y = \pm 1$, that is, on the wavefront $x = |1 \pm \tau|$. Regular solutions can be obtained by appropriate choices of A and B . We plot in fig.(7) a regular solution $h_1(y)$ for $B = 1$.

We obtain from eqs.(6.8) and (6.10) the physical fields:

$$\psi = \pm c_s C y h_1(y) \quad , \quad \phi = \ln \left\{ \frac{C}{x^2} [1 - C h_1(y)] \right\} . \quad (6.11)$$

It is important to notice that this perturbative development fails at short distances ($y \rightarrow 0$) where the density is not small anymore.

C. Fluctuations around a soliton-like solution

We intend to assess the stability of the solution (6.6). By stability we mean that the growth of the fluctuations should be slower than the growth of the background.

We compute here the explicit form of the radial fluctuations around the soliton-like solution described by eq.(6.6). The collapsing filament case is studied. We define the two independent variables:

$$y = \frac{x}{1-\tau}, \quad z = 1-\tau. \quad (6.12)$$

We consider the perturbative expansion

$$\phi(x, \tau) = \phi_0 + \epsilon f(y, z), \quad \frac{d\psi}{dx}(x, \tau) = \frac{d\psi_0}{dx} - c_s \epsilon g(y, z). \quad (6.13)$$

We can then linearize the evolution equations and we find

$$\sqrt{C}y \frac{\partial^2 g}{\partial y^2} - yz \frac{\partial^2 g}{\partial y \partial z} - (-\sqrt{C} + y) \frac{\partial g}{\partial y} - z \frac{\partial g}{\partial z} - g = y \frac{\partial^2 f}{\partial y^2} + \frac{\partial f}{\partial y} + \sqrt{C}f, \quad (6.14)$$

$$-\sqrt{C} \frac{\partial f}{\partial y} + z \frac{\partial f}{\partial z} + \frac{\partial g}{\partial y} = 0. \quad (6.15)$$

These equations are homogeneous in z so their solutions can be written as a sum of solutions of the type:

$$f(y, z) = f(y) z^\alpha, \quad g(y, z) = g(y) z^\alpha, \quad \alpha \in \mathbb{C}. \quad (6.16)$$

Inserting these expressions in eqs.(6.14) and (6.15) and eliminating g , gives an equation for f :

$$x(C-1) f''' + [2(C-1) - (2\alpha+1)\sqrt{C}x] f'' + [-(4\alpha+3)\sqrt{C} + \alpha(\alpha+1)x] f' + 2(\alpha+1)\alpha f = 0. \quad (6.17)$$

This equation can be integrated in the general case. However, according to the transformation (6.7) we can choose the case $\sqrt{C} = 1$. In this case the solutions take the following form:

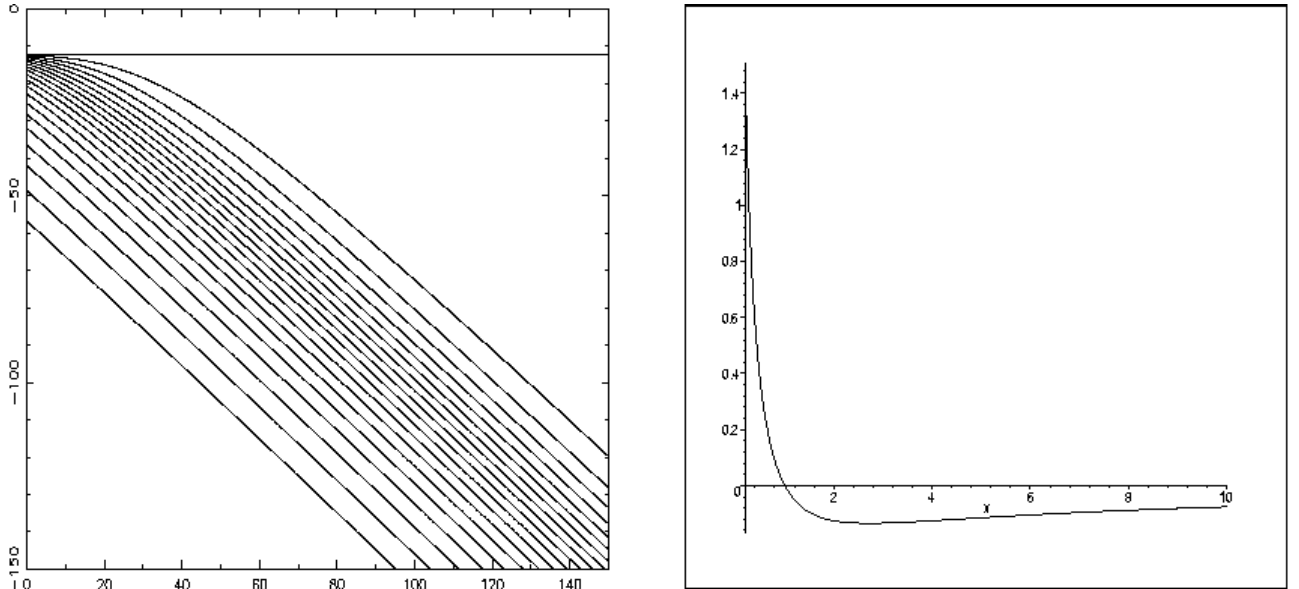


FIG. 7. On the left solutions to eq.(6.5) are plotted for various initial conditions. On the right the function h_1 is plotted for $B = 1$.

$$f(y) = B_1 \Phi(\lambda_1, \nu_1, \beta y) + B_2 y^\gamma \Phi(\lambda_2, \nu_2, \beta y) . \quad (6.18)$$

where,

$$\lambda_1 = 2 , \quad \nu_1 = 2 + \frac{1}{1 + 2\alpha} , \quad \lambda_2 = \frac{2\alpha}{2\alpha + 1} , \quad \nu_2 = \frac{-1}{2\alpha + 1} , \quad (6.19)$$

$$\beta = \frac{\alpha(\alpha + 1)}{2\alpha + 1} , \quad \gamma = -1 - \frac{1}{2\alpha + 1} . \quad (6.20)$$

Here $\Phi(\lambda, \nu, y)$ stands for the confluent hypergeometric function. It is regular at $y = 0$ and grows exponentially for $y \rightarrow \infty$. Expression (6.18) is degenerate for $\alpha = -\frac{1}{2}$:

$$\alpha = -\frac{1}{2} , \quad f(y) = \frac{B}{1 + \frac{y}{4}} . \quad (6.21)$$

According to (6.16), it diverges when the time τ reaches 1.

Another degenerate case is $\alpha = -1$,

$$\alpha = -1 , \quad f(y) = y \left[\ln \left(\frac{B_1}{y} \right) + 1 \right] + B_2 . \quad (6.22)$$

Interestingly, $Re(\alpha) \in [-1, -\frac{1}{2}]$ are the only values of α where the fluctuations are regular at $y = 0$. But again the fluctuations diverge for $\tau \rightarrow 1$.

Since the fluctuations are ill-behaved for $y \rightarrow \infty$ and often at $y = 0$, we resort to the same method as in the singular isothermal sphere. We define a large distance cutoff X and a small distance cutoff δ for y and we set the fluctuation to zero on these walls. It should be noted that these walls move with the soliton, and that they cannot be considered as physical since the constant component of the background velocity field flows through the walls. However, those cutoffs allow us to search for fluctuations as eigenmodes in the same way we did for isothermal spheres. These modes appear for special values of α defined here again by the cancellation of a determinant:

$$\Phi(\lambda_1, \mu_1, \beta\delta) X^\gamma \Phi(\lambda_2, \mu_2, \beta X) - \Phi(\lambda_1, \mu_1, \beta X) \delta^\gamma \Phi(\lambda_2, \mu_2, \beta\delta) = 0 \quad (6.23)$$

These cancellations must be investigated in the complex plane for α and for various values of $\frac{X}{\delta}$. The results appear on fig. 8. The main result is that modes with $Re(\alpha) < 0$ exist for all values of $\frac{X}{\delta}$ investigated. These modes have a faster growth than the background. Besides, $\frac{X}{\delta} \sim 4.5$ is a special value for the radial size of the system. Below this value all the unstable modes have the following time behaviour

$$(1 - \tau)^{\alpha_1} \cos[\alpha_2 \ln(1 - \tau) + \phi]$$

that is, growing oscillations. Above this value $\frac{X}{\delta} \sim 4.5$ two modes appear that have a pure power law behaviour on time. These modes have larger exponents than the others, that is to say they grow faster. Moreover, just above this critical value, the exponent in the power law seems to go to $-\infty$, which indicates a strong instability.

We must keep in mind the fact that this is a partial analysis. Indeed our fluctuations are invariant along the z symmetry axis. This means that they have an infinite mass. If the size of the system along the z symmetry axis were bounded and fluctuations with r and z dependence computed, a stable region would certainly appear for small enough sizes. We believe that the value $\frac{X}{\delta} \sim 4.5$ is actually connected to the onset of a *radial* instability, while below this value the growth of the modes is due to the axial infinite size of the fluctuations.

VII. CONCLUSIONS

In the first part of this work we have described a general method to study the dynamical stability of stationary configurations of self-gravitating fluids and applied it to the isothermal spheres. The interest of this method is that it can be applied to any stationary field. Moreover, it is perfectly able to handle viscosity. We have applied this dynamical stability analysis to a stationary solution, the isothermal sphere. In this case we have found a series of sizes ($X_{c_n} \sim 10.7^n$) associated with the appearance of instable modes. The size associated to the first instable mode matches the critical size found in the thermodynamical theory. Moreover we have shown that the value of these sizes are independent of the Reynolds number.

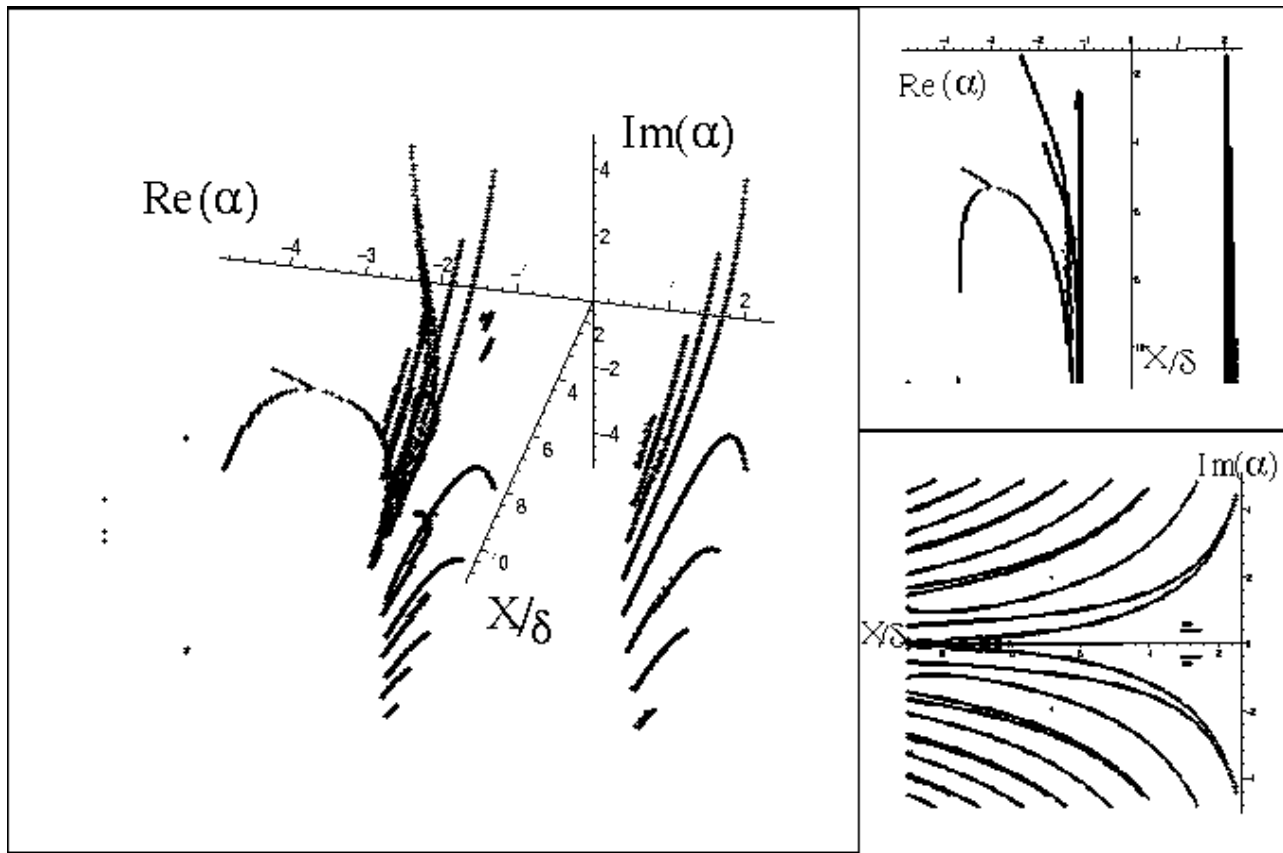


FIG. 8. Spectrum of modes around solution 6.6 for a continuous range of values of $\frac{R}{\delta}$. The real and imaginary parts of α are plotted against $\frac{R}{\delta}$.

In the second part we studied exact dynamical solutions. We have presented elements of a soliton theory for a self-gravitating perfect isothermal fluid with axial symmetry. This method provides new dynamical exact solutions. We have analyzed the stability of one of these solutions, a collapsing filament, with a method similar to the method used for the isothermal sphere. Here again we have found that a critical radial size appears to define two regimes. Above this size the system is unstable. Below, it is weakly unstable and may in fact be stable if the axial size of the system were bounded.

These two studies are complementary descriptions of the dynamics of the self-gravitating fluid. One description deals with a stationary background and the other with a dynamical one. Although the first obeys a spherical symmetry and the second obeys an axial symmetry, they are closely connected by their structure. Indeed, the density field of eq.(6.6) is the sum of two terms: $\ln(2/\mu^2 r^2)$ (identical to the stationary spherical solution) and a second term, $\ln \left[\frac{\sqrt{C}}{1 \pm \mu c_s t} \right]$, function of the soliton-like variable alone. In the stationary case, the instability appears when a mode is growing; in the dynamical case it appears when a modes is growing faster (or decaying slower) than the evolving background solution. In this respect, the stability of the solution is ruled in both cases by Jeans-like instabilities whose emergence depends only on the size of the system. We showed that the existence of a critical size does not only apply to stationary solutions but to dynamical solutions as well.

Finally, we would like to add that it is probably possible to give a more general formulation of the soliton-type equations of the system, like that given in ref. [13] in the one dimensional-case. For example, the choice of the soliton variable in our work, eq.(6.2), is probably a particular case of a more general change in the variables. In any case, the soliton methods provide a powerful approach to self-gravitating fluid dynamics which certainly deserves more attention.

- [1] Ya. B. Zeldovich and I. D. Novikov, 'Relativistic Astrophysics', Univ. of Chicago Press, 1983.
W. C. Saslaw, 'Gravitational Physics of Stellar and Galactic Systems', Cambridge U. Press, 1987.
- [2] V. A. Antonov, Vest Lenin Univ, **7**, 135 (1962)
- [3] D. Lynden-Bell and R. Wood, MNRAS, **138**, 495-525 (1968)
- [4] G. Horwitz and J. Katz, ApJ, **222**, 941-958 (1978)
- [5] S. Chandrasekhar, *An introduction to the study of stellar structure*, New York, Dover, (1939)
- [6] T. Padmanabhan, Phys Rep, **188**,5, 285-362 (1990)
- [7] L. Landau and E. Lifchitz, Mécanique des Fluides, Eds. MIR, Moscou 1971.
- [8] L. Hernquist and N. Katz, ApJ Sup, **70**, 419 (1989)
- [9] H. J. de Vega, N. Sánchez and F. Combes, Nature, **383**, 56 (1996), Ap. J. **500**, 8 (1998).
- [10] H. J. de Vega, N. Sánchez and F. Combes, Phys. Rev. **D54**, 6008 (1996).
- [11] B. Semelin, H. J. de Vega, N. Sánchez and F. Combes, Phys. Rev. **D59**, 125021, (1999)
- [12] H. J. de Vega and N. Sánchez, hep-th/9903236.
- [13] G. Gözt, Class Quantum Grav, **5**, 743-765 (1988)
- [14] S. Inutsuka and S. M. Miyama, Ap J, **388**, 392-399 (1992)